



## Application of Euler-Poincaré Characteristic in the Prediction of Permeability of Porous Media

Yibo Zhao<sup>1,2</sup>

<sup>1</sup>School of Mathematical Sciences, University of Electronic Science and Technology of China, Chengdu, Sichuan 611731, China

<sup>2</sup>School of Data and Computer Science, Shandong Women's University, Jinan, Shandong, 250300, China

### ABSTRACT

In this paper, a new model is proposed to predict the permeability of porous media. This model introduces the Euler-Poincaré Characteristic (Euler Number), a parameter that reflects the connectivity of porous media. Using fractal and percolation theory, we establish a permeability model as a function of critical radius, porosity and Euler number. In order to relate the result to the Euler number, we introduce the Connectivity Function to calculate the critical aperture in the percolation theory, then calculate the percolation threshold value, and establish the relationship between the percolation threshold and the Euler number. The validity of the model is verified by the structural data of 12 rock samples. For selected rock samples, the proposed model results are compared with the Daigle's method and LBM. The results show that the permeability values obtained by the model are consistent with the LBM experimental data and are higher than those predicted by the Daigle's model.

**KEY WORDS:** Permeability, Euler Number, Percolation theory, Porous media

### 1 INTRODUCTION

SINCE the 1940s, estimating the permeability of porous media from microscopic and macroscopic soil properties has been an area of intense research. The early research model was developed based on a capillary method that creates a porous media model by replacing the actual interconnected pore paths with equal-length straight cylindrical bore tubes (e.g., Purcell, 1949; Child and Collis-George, 1950). Based on the model of Purcell (1949) and Childs and Collis-George (1950), Marshall (1957, 1958) proposed to estimate the permeability of porous media based on the measured capillary pressure curve. In recent years, the development of digital image processing technology has also played a very important role in promoting the study of porous media. Liu et al. (2018) used high-resolution remote sensing image technology for multi-phase oil tank identification to study the permeability of porous media. Gharsallah et al. (2018) proposed a method for the enhancement of heterosexual images. The method can be used to analyze the internal structure of porous media. Ganesh et al. (2017) used an enhanced adaptive fuzzy K-means

algorithm to segment the image and can be used to study porous media.

Over the past 30 years, based on the relationship between capillary pressure and pore radius proposed by Washburn (1921), mercury intrusion porosity measurement (MIP) (Giesche, 2006) has become an effective technique for characterizing porous media. Based on this, Davudov and Moghanloo (2016) and Davudov et al. (2016) used the mercury injection capillary pressure (MICP) method to obtain basic data of shale samples. MICP measurement is one of the best techniques to provide direct information about the pore throat which is a key parameter for the connectivity of porous media. Several researchers have been studying the use of MICP data to predict permeability, where the Katz and Thompson (1986, 1987) methods are the methods we use to calculate permeability, and our new equation is based on that method. Katz and Thompson (1986) have studied that fluid flow and conductance through a porous medium are percolation processes, and permeability may be related to the conductivity and critical pore size of the porous medium.

Katz and Thompson (KT) model is given by:

$$k = \frac{1}{c} \frac{\sigma_b}{\sigma_w} r_c^2 = \frac{1}{c} \frac{r_c^2}{F} \quad (1)$$

where  $k$  is permeability of porous media,  $\sigma_b$  is bulk electrical conductivity,  $\sigma_w$  is saturating fluid electrical conductivity,  $r_c$  is critical pore radius,  $F$  is electrical formation factor and  $c$  is a constant which is function of pore shape. They believe that the critical pore size can be estimated by mercury intrusion into porosity measurement data, and the inflection point on the mercury intrusion curve corresponds to the critical pore size. In the KT model, the formation factor and the critical pore radius are functions of hydraulic conductivity, which has been implicitly expressed.

In order to improve the predictability of flow and transport in porous media, it is necessary to study the geometrical factors that control the distribution and velocity of the fluid in the porous media. Because the geometry of the pore space is difficult to visualize and quantify, finding the dominant factor that affects permeability is a difficult task. Through microphotography, the geometry of the pore space can be described, and this information must be appropriately included in the structural properties of the pore network. Vogel and Roth (2001) measured the geometry of the pore space through continuous slicing and generated the same network model as the pore size and pore connectivity obtained by image analysis. Based on the imaging aperture distribution and pore connectivity, they can demonstrate that connectivity has a significant impact on permeability, relative hydraulic conductivity, and solute transport properties (Vogel, 2000).

In order to include the factors affecting pore connectivity in the permeability model, several equations have been proposed. The most commonly used model is proposed by Kozeny (1927). Carman (1937) improved the model and formed the Kozeny-Carman relationship (KC equation):

$$k = \frac{\phi^3}{c(1-\phi)^2 S^2} \quad (2)$$

where  $k$  is permeability,  $c$  is Kozeny constant,  $S$  is specific surface area based on solid volume. Bear (1972) and Kaviany (1995) further modified the KC equation as:

$$k = \frac{\phi^3}{K(1-\phi)^2 S^2} = \frac{\phi^3}{36K(1-\phi)^2} d^2 \quad (3)$$

where  $k=c\tau^2$  is KC constant,  $\tau$  is the tortuosity,  $d=6/S$  is the mean diameter for the hypothetical spherical solid particles with the same specific surface area  $S$ . Although the KC equation is accepted and used widely,

there are many limitations since its introduction. This equation is a semi-empirical formula, and KC has also been shown not to be a constant, which may be related to the porosity of the porous medium (Kaviany, 1995). In order to improve the accuracy of the permeability prediction, the KC model has different versions. Pape et al. (2000) proposed permeability prediction model based on fractal theory:

$$k = \frac{r_g}{8} \frac{\phi}{T^2} \left( \frac{2\phi}{3T^2(1-\phi)} \right)^{\frac{2}{D_f-1}} \quad (4)$$

where  $k$  is permeability of porous media,  $r_g$  is grain radius,  $D_f$  is fractal dimension,  $\phi$  is porosity and  $T$  is tortuosity parameter.

Although the literature on porous media permeability has been growing rapidly over the past few decades, it is not yet fully understood how the transport properties of liquids passing through porous media are related to microscopic geometry, and even single-phase flow is not fully understood. Due to the complexity of rock pore structure, it is difficult to fully describe the permeability of pore rock using the above mathematical model. The relationship between the connectivity of the pore structure and the permeability of the rock is not clear, and the permeability of the pore rock is extremely random. This makes the prediction of permeability very difficult. Here we introduce the fluid topology, expressed by the Euler-Poincaré Characteristic (Euler Number), as the shape measurement of the porous medium. The Euler Number is the most basic shape parameter that reflects the connectivity of the porous medium.

It can provide a close relationship between topological characterization of pore connectivity and macroscopic formula of permeability in porous media. Establishing the relationship between the permeability and the Euler number makes it possible to accurately and reasonably predict the rock permeability of different characteristics.

In this study, we mainly discussed the use of Euler numbers, which are parameters that reflect the connectivity of porous media, to predict the permeability of porous media. Specifically, we use fractal and percolation theory to analyze the relationship between pore connectivity and permeability. The main purpose of this study is to show the relationship between the Euler number and the permeability of the porous media. Compared with the conventional prediction model, the calculation accuracy has been significantly improved.

## 2 PORE SYSTEM CHARACTERISATION

WHEN a 3D model of porous media (such as a 3D digital core image) exists, it is necessary to extract the geometry of the pore system. Here, we use the method proposed by Jiang et al.(2007). In short, it is the "ball

fitting" method. This method is a non-overlapping method that divides the pore space into spatially sphere-equivalent components. The geometric and topological properties of many porous media such as pore size distribution, coordination number, and Euler characteristics can be easily calculated based on this method.

**2.1 Pore-size quantification**

Because the microscopic geometry of porous media is very complex and the spatial shape is irregular, it is difficult to have an accurate definition of the "porosity" of porous media. Based on the minimum of the average radius of curvature (or hydraulic radius) of porous media, Dullien (1992) proposed the concept of "pore neck". However, Zhao et al. (1994) pointed out that this method will leave part of the pore neck missing, while other non-aperture areas may be incorrectly marked as the pore neck, unless the section is narrowed in sufficient directions on the image data set search. Jiang et al. (2012) adapted and extracted the basic idea of each pore from the pore space in descending order of pore radius, and improved the combination of "ball adaptation" and "backbone" approaches. In this fitting algorithm, pores are extracted from the 3D digital image of the porous medium in a stepwise manner according to the pore size. Based on the relationship between porosity and pore size (Mudder, 1996) and the improvement of Jiang et al.(2011), the following expression can be used to estimate the maximum possible pore radius:

$$r_m = \frac{1}{3} \left( \frac{3v\phi}{4\pi} \right)^{\frac{1}{3}} \tag{5}$$

where  $r_m$  is the upper-limit radius of pore size,  $\phi$  is the porosity,  $v$  is the volume of the 3D image. In order to measure the maximum sphere size of the aperture, the template spheres are required as shown in Fig 1.

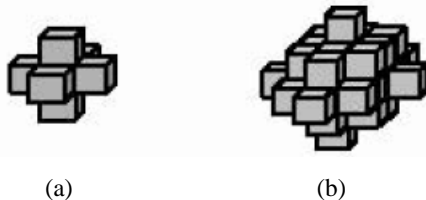


**Figure 1.** The template discrete spheres. (a), (b): spheres of radius 1, 2 respectively.

After the pores have been determined by the above process, they are removed from the pore space using a cubic cut method to avoid overlapping with later extracted pores.

**2.2 Euler-Poincaré Characteristic**

The Euler-Poincaré Characteristic (Euler Number) is a well-known measure of the connectivity of the

reactive pore media. In three dimensions, it is the number of connected components minus the number of tunnels plus the number of enclosed cavities. Since the space is discrete in the binary image, it is necessary to replace the continuous average with a discrete average, and the connectivity of the image must be measured on the grid. Depending on the shape of the lattice used (e.g., cubic or hexagonal) and the manner in which pores in the interior of the porous media are connected (e.g., 6- or 26-connected on a cubic lattice), different methods can be used. We choose to use cubic grid and 26 connectivity.

Following Kong's discussion (1989), assume that the representation of 3D binary image  $P$  is  $(V, \alpha, \beta, B)$ , where  $V$  is a subset of all cubic grid points in  $Z^3$ ,  $B$  is a set of all object points (called foreground) in  $V$ , and  $V - B$  is the non-object (i.e. background),  $\alpha$  and  $\beta$  are two adjacency for the foreground and the background, respectively, the adjacency pair of (26,6) will be discussed for simplicity in this paper.

For a point  $x = (x_1, x_2, x_3) \in Z^3$ , the neighbourhoods are defined in the following (See Figure.2):

i) The 6-neighborhood:

$$N_6(x) = \{y \in Z^3 \mid |y_1 - x_1| + |y_2 - x_2| + |y_3 - x_3| \leq 1\}; \tag{6}$$

ii) The 26-neighborhood:

$$N_{26}(x) = \{y \in Z^3 \mid \text{Max}(|y_1 - x_1|, |y_2 - x_2|, |y_3 - x_3|) \leq 1\}; \tag{7}$$

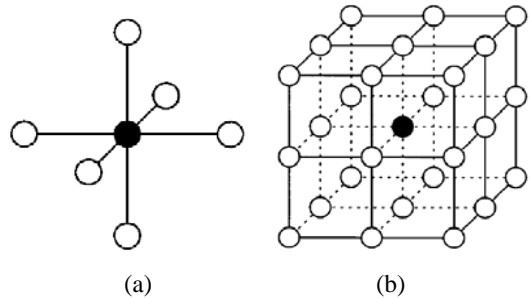


**Figure 2.** The types of neighbourhoods containing (a) 6 6-neighbours, (b) 26 26-neighbours x (black circle), respectively.

Saha and Chaudhuri (1995) established a recursive relationship based on the direct neighborhood classification to calculate the Euler number. However, the algorithm requires a look-up table of 226 entries and 64M bytes of memory. Therefore, the resource cost of this algorithm is still too high. Similar to Saha's method, Jiang's algorithm (2011) (Eq.8) is based on calculating the black component, the local variation of the number of tunnels and cavities, but the algorithm no longer uses any kind of tables, but provides a relationship based on the relationship between the number of topologies and the three Betty numbers.

**Algorithm** (Calculation of the Euler number):

(a)  $\chi(V, \alpha, \beta, B) = 0$  if  $B = \phi$ ;

(b) for any point  $p \in B$ , we have

$$\chi(V, \alpha, \beta, B) = \chi(V, \alpha, \beta, B - \{p\}) + T_6(p) - T_{26}(p). \quad (8)$$

where  $T_6(p)$  is solid topological number and  $T_{26}(p)$  is pore topological number of  $p$ ,  $\chi$  is the Euler number. In order to eliminate the effect of sample size on the Euler number, we use the specific Euler Number  $\chi_V$ , which is the Euler number  $\chi$  divided by the sample volume  $V$ .

### 3 PERCOLATION THEORY AND CRITICAL PATH ANALYSIS

THE percolation theory is one of the best methods to study the connected paths in disordered media such as rock matrix. It can simulate pore systems with low connectivity (Hunt, 2001; Hunt and Ewing, 2009). The pore volume portion is occupied for the first time to form a connecting cluster. The pore volume fraction occupied at this time is called the critical percolation threshold. The percolation threshold is an important parameter, because at this point, the connectivity of the porous medium undergoes drastic changes. According to percolation theory, the flow of a given phase occurs only when the saturation of the phase exceeds a certain threshold (percolation threshold,  $p_c$ ). The percolation threshold depends on the degree of connectivity of the pore system and the well connected pore system has a lower percolation threshold.

Critical path analysis (CPA) is a special technique based on percolation theory, which shows good application prospects in determining permeability in porous media such as rocks and soil (Friedman and Seaton, 1998; Hunt, 2001; Skaggs, 2011). According to the CPA, it is assumed that the inhomogeneous porous media consists of communicating paths (pores) with different conductances, that is, different transport flow capabilities. The conductance is related to the pore size, with larger pores having larger conductance. Most of the flow through the porous media occurs on high-conductivity interconnected paths that make up a portion of the total available for flow. Therefore, macroscopic flows are determined by the low conductivity constraints that occur along these paths (Hunt, 2001).

In the present work, a fractal description of the pore space is used to parameterize the pore size volumetric probability density function. Euclidean geometry uses integer dimensions to describe ordered objects, such as points, curves, surfaces, and cubes with dimensions of 0, 1, 2, and 3, respectively. Associated with each dimension is the measurement of the object, such as length, surface area, and cube volume. However, many objects found in nature, such as rough surfaces, coastlines, rocks, mud, etc., are disordered and irregular. Because length, area and volume are related to each other, they do not follow Euclidean descriptions (Mandelbrot, 1982). These objects are called fractals. The dimensions of these objects are non-integer and are

defined as fractal dimensions. The use of fractals to describe the geometry of the pore space means that the pore system exhibits a statistical self-similarity (Tyler, 1990).

Let  $W(r)$  be the probability density function of pore sizes in the medium, where  $r$  represents the pore radius. Hunt and Ewing (2014) develop a normalized form for pore radii:

$$W(r) = \frac{3-D}{r_m^{3-D}} r^{-1-D}, \quad r_0 \leq r \leq r_m \quad (9)$$

where  $D$  is the fractal dimension,  $r_0$  is the smallest pore radii, and  $r_m$  is the largest.

The total porosity derived from Eq.9 is

$$\phi = \frac{3-D}{r_m^{3-D}} \int_{r_0}^{r_m} r^3 r^{-1-D} dr = 1 - \left( \frac{r_0}{r_m} \right)^{3-D} \quad (10)$$

So that

$$D = 3 - \frac{\lg(1-\phi)}{\lg(r_0/r_m)}. \quad (11)$$

Based on the Porosity Solid Fractal (PSF) model, Daigle (2016) proposed a volumetric probability density function  $f(r)$  for an aperture.

$$f(r) = \frac{\beta}{\phi} \frac{3-D}{r_m^{3-D}} r^{2-D}, \quad r_0 \leq r \leq r_m \quad (12)$$

where  $\phi$  is porosity,  $\beta$  is the ratio of pore volume to the sum of the pore and solid volumes in the fractal model. As Davud and Rouzbeh (2018) state, if it is assumed that  $\beta \approx \phi$ , then Eq.12 can be simplified as:

$$f(r) = \frac{3-D}{r_m^{3-D}} r^{2-D}, \quad r_0 \leq r \leq r_m \quad (13)$$

According to CPA, the critical pore size  $r_c$  of a porous medium can be defined as

$$p_c = \int_{r_c}^{\infty} f(r) dr = \frac{3-D}{r_m^{3-D}} \int_{r_c}^{r_m} r^{2-D} dr = 1 - \left( \frac{r_c}{r_m} \right)^{3-D} \quad (14)$$

Which may be rearranged as

$$r_c = r_m (1 - p_c)^{\frac{1}{3-D}} \quad (15)$$

where  $p_c$  is percolation threshold.  $r_m$  is the largest pore size of the medium. Eq.14 shows that if the pore size is gradually occupied from the maximum, the percolation threshold will be reached when the pore size  $r_c$  is occupied.

Katz and Thompson (KT) model (Eq.1) are the model that we use to calculate permeability of porous medium. The surface conductivity is ignored and the formation factor  $F$  can be represented by the percolation threshold (Ghanbarian et al., 2014; Daigle, 2016):

$$\frac{1}{F} = \left[ \frac{\phi(1-p_c)}{1-\phi p_c} \right]^m \quad (16)$$

The universal scaling exponent  $m$  is equal to 2 in three dimensional systems (Stauffer and Aharony, 1992). According to the above arguments, Eq.1 and Eq.16 are used to obtain the permeability calculation formula:

$$k = \frac{r_c^2}{c} \frac{1}{F} = \frac{r_c^2}{c} \left[ \frac{\phi(1-p_c)}{1-\phi p_c} \right]^m \quad (17)$$

As can be seen from Eq.17, the permeability of porous media can be calculated only by knowing the aperture distribution, porosity and percolation threshold. Numerical simulations of digital rock samples from different types of rock (e.g. carbonate, sandstone, consolidation and loose rock) support  $c=8$  in the KT model (Bauget et al., 2005a, 2005b; Knackstedt et al., 2006).

#### 4 MATERIALS AND METHODS

DAIGLE (2016) used a Micromeritics Autopore III instrument to determine the percolation threshold by comparing pore size distributions and mercury injection capillary pressure (MICP) measurements. The MICP data for the marine muds were previously reported by Daigle in table 1. MICP measurements can be described using bond percolation theory, which forms a sample-spanning cluster of connected mercury-filled pores when the volume fraction of the mercury-filled pore system is equal to  $p_c$ . The percolation threshold can be considered as the point of maximum slope in the graph of the cumulative volume of mercury intrusion versus the Mercury pressure (Katz and Tompson, 1987), but they stated that it will cause a large measurement error because the injection rate is too fast. Therefore, in this case, the critical aperture  $r_c$  calculated using Eq.15 will cause greater error. Here  $r_c$  is the critical pore radius, which corresponds to the radius of the largest sphere that can permeate through the pore space of the sample, so that an interconnected path can be formed from one side of the system to the other. And the radius that will not be encountered on this path is less than the aperture of the  $r_c$  (Robins, V. et al (2016), Davud Davudov et al (2018)). If pores are occupied progressively starting with the largest pores, the percolation threshold will be reached when pores of

size  $r_c$  are occupied (Hugh Daigle, 2016). Motivated by the observation, valid in various stochastic processes, the Euler characteristic vanishes near the percolation threshold (Scholz, C. et al (2012)). Therefore, when the Euler number disappears, the corresponding aperture size is close to the critical pore radius of the pore medium. The turning point (the zero crossing) from the Connectivity Function curve can be defined as critical pore size or critical pore diameter.

From the statistical analysis of the data in Table 1, the permeabilities and percolation thresholds and porosity satisfy the following power relationship. Figure 3 shows the power relationship for 15 rock samples.

$$\frac{ck_{meas}}{r_c^2} = \left[ \frac{\phi(1-p_c)}{1-\phi p_c} \right]^{1.898} \quad (c=8) \quad (18)$$

**Table 1. Sample data. Sample names starting with numbers are Japanese marine mudstones (Daigle, H. 2016).  $p_c$  is the percolation threshold calculated by comparing pore size distributions with mercury injection capillary pressure measurements (MICP).  $r_c$  is the critical pore radius calculated by Eq.15,  $k_{meas}$  is measured permeability of rock sample,  $\phi$  is porosity.**

Sample	$\phi$	$k_{meas}(um^2)$	$p_c$	$r_c(um)$
1	0.69	0.0028	0.49	0.28
2	0.67	0.002	0.4	0.23
3	0.68	0.0018	0.32	0.2
4	0.53	0.00058	0.3	0.12
5	0.71	0.0048	0.54	0.36
6	0.72	0.0021	0.48	0.22
7	0.58	0.0005	0.29	0.12
8	0.57	0.00079	0.29	0.15
9	0.66	0.0036	0.2	0.29
10	0.62	0.0022	0.45	0.28
11	0.57	0.00091	0.26	0.17
12	0.52	0.00078	0.3	0.18
13	0.46	0.0013	0.47	0.33
14	0.21	0.31	0.34	11
15	0.18	0.17	0.49	12

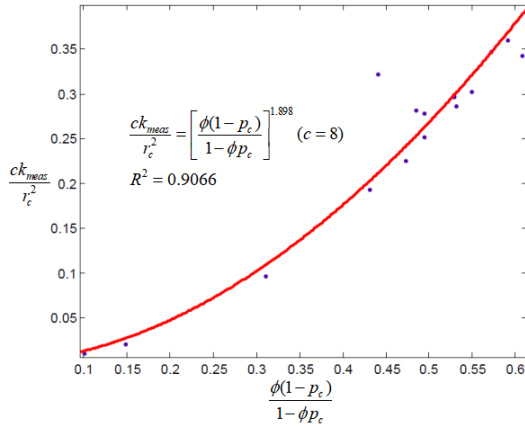


**Figure 3.** The permeabilities and percolation thresholds and porosity satisfy power relationship, with correlation  $R^2=0.9066$ .

The exponent 1.898 of the power law is not greatly different from the value of 2 (Ghanbarian et al. (2014)), the root mean square error is 0.03468.

Twelve 3D tomography rock images (Figure 4) were selected for the study. The properties of all samples are given in Table 2. Using the data of Table 2, we also analyzed the power ratio relationship between permeability and percolation threshold and porosity :

$$\frac{ck_{LB}}{r_c^2} = \left[ \frac{\phi(1-p_c)}{1-\phi p_c} \right]^{1.82} \quad (c=8) \quad R^2 = 0.6581 \quad (19)$$

where the critical pore radius  $r_c$  is the zero crossing point of Connectivity functions (Figure 4), The permeability  $k_{LB}$  is calculated by Lattice Boltzmann method (LBM), the percolation threshold  $p_c$  is calculated by Eq.14. Although there are scatters, the exponent 1.82 of the power law is also not greatly different from the value of 2, the root mean square error is 0.02897(Eq. 18) < 0.03468(Eq.19). This shows that the method of determining critical apertures by using the zero crossing point of Connected Functions is correct.

The micro fluid experiment and the lattice Boltzmann simulation show that there is a power law distribution between the connectivity of porous media and the Euler characteristics. Therefore, we speculate that there is a certain relationship between the percolation threshold and the Euler number. In order to obtain a representative empirical formula to predict the percolation threshold of porous media, the permeability of 12 rock samples was tested by LBM. The sample is listed in Table 2. The new empirical equation is obtained as follows:

$$p_c = a \cdot e^{b\chi_v} + c \quad (20)$$

where  $\chi_v$  is the specific Euler characteristic,  $a, b, c$  are constants.

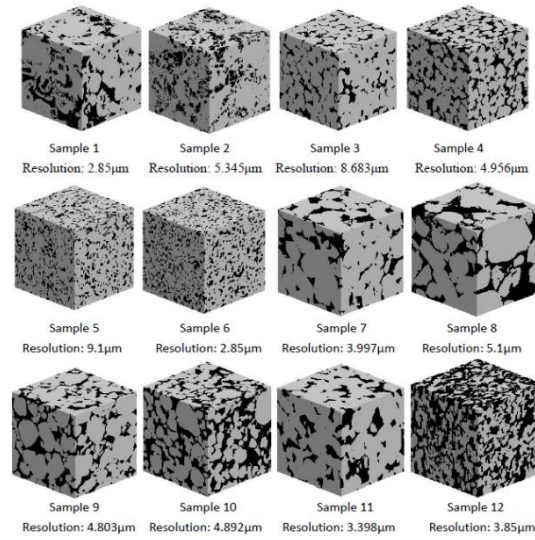


**Figure 4.** 12 3D tomography rock images of samples

Figure 6 shows the percolation threshold as a function of the specific Euler number for all 12 rock samples (Table 2). We observe that percolation threshold  $p_c$  is relatively highly correlated to specific Euler number, with correlation coefficient  $R^2=0.6695$ . Therefore, on the bases of Eq.17, and Eq.20 the permeability  $k$  prediction formula can be expressed as:

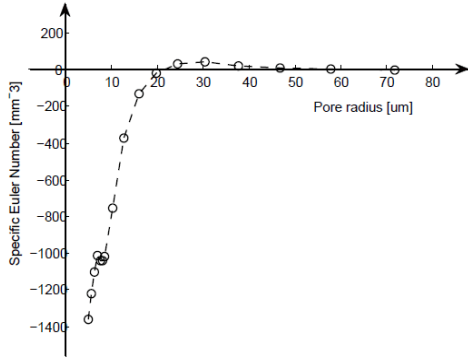
$$k = \frac{r_c^2}{c} \left[ \frac{\phi(1-a \cdot e^{b\chi_v} - c)}{1-\phi(a \cdot e^{b\chi_v} + c)} \right] \quad (21)$$

Eq. 21 reflects the relationship between Euler characteristics and permeability of porous media. In order to compare the accuracy of different permeability models in the permeability estimation, we compare the results of different model calculations with the results calculated by the lattice Boltzmann method using the data in Table 2. Flowing Ghanbarian et al.(2017) the root mean square log-transformed error (RMSLE) is calculated as follow:

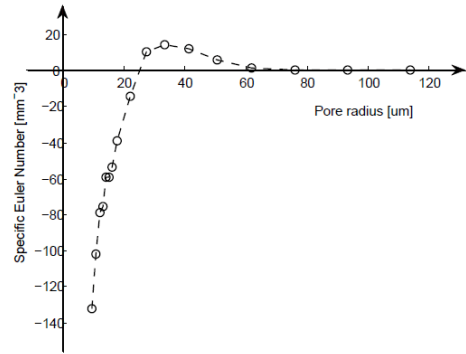
$$\text{RESLE} = \sqrt{\frac{1}{N} \sum_{i=1}^N [\log(k_{LB}) - \log(k_{cal})]^2} \quad (22)$$

where  $N$  is the number of values,  $k_{LB}$  is permeability calculated by LBM and  $k_{cal}$  is the calculated (estimated) permeability.

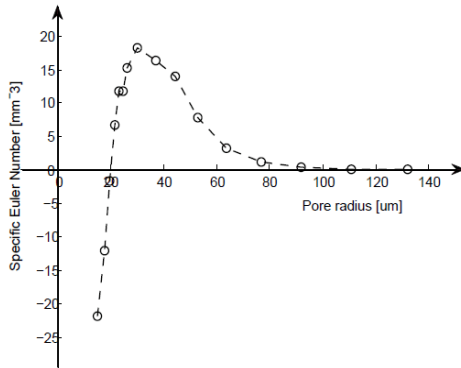
According to Table 3, apart from sample 2, there is only a slight difference between  $k_{cal}$  and  $k_{LB}$  for all other sandstone samples. Because the permeability measured by experiments is very difficult, it is not uncommon for the same sample to measure 1-2 orders of magnitude in different ways. As a result, Eq.21 is reliable to calculate permeability and selection of Eq.17 as the sample permeability to derive the new equation is appropriate.



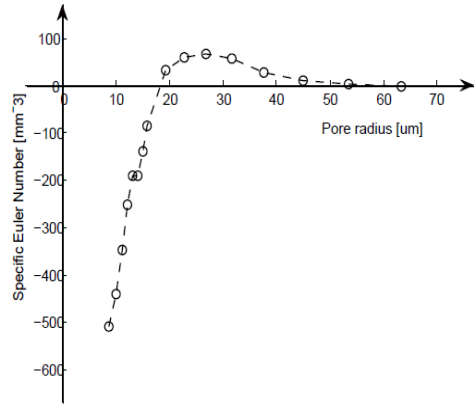
Sample 1



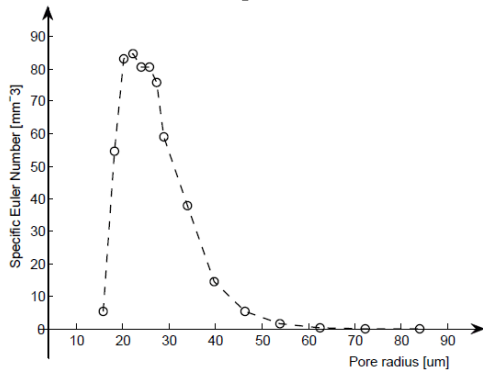
Sample 2



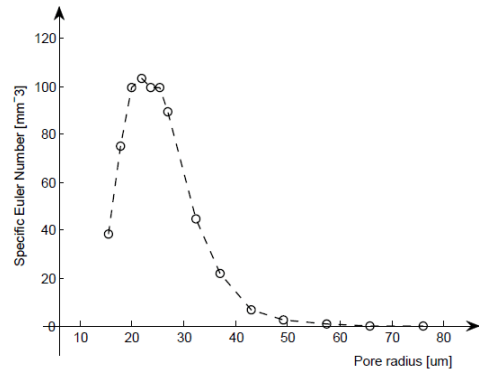
Sample 3



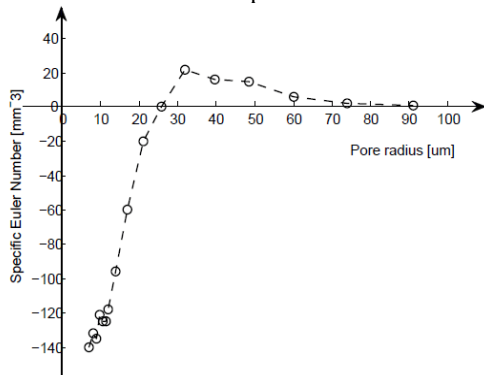
Sample 4



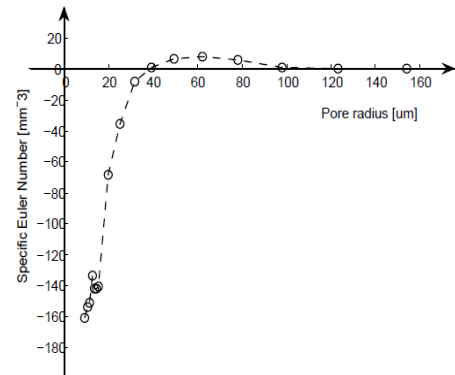
Sample 5



Sample 6



Sample 7



Sample 8

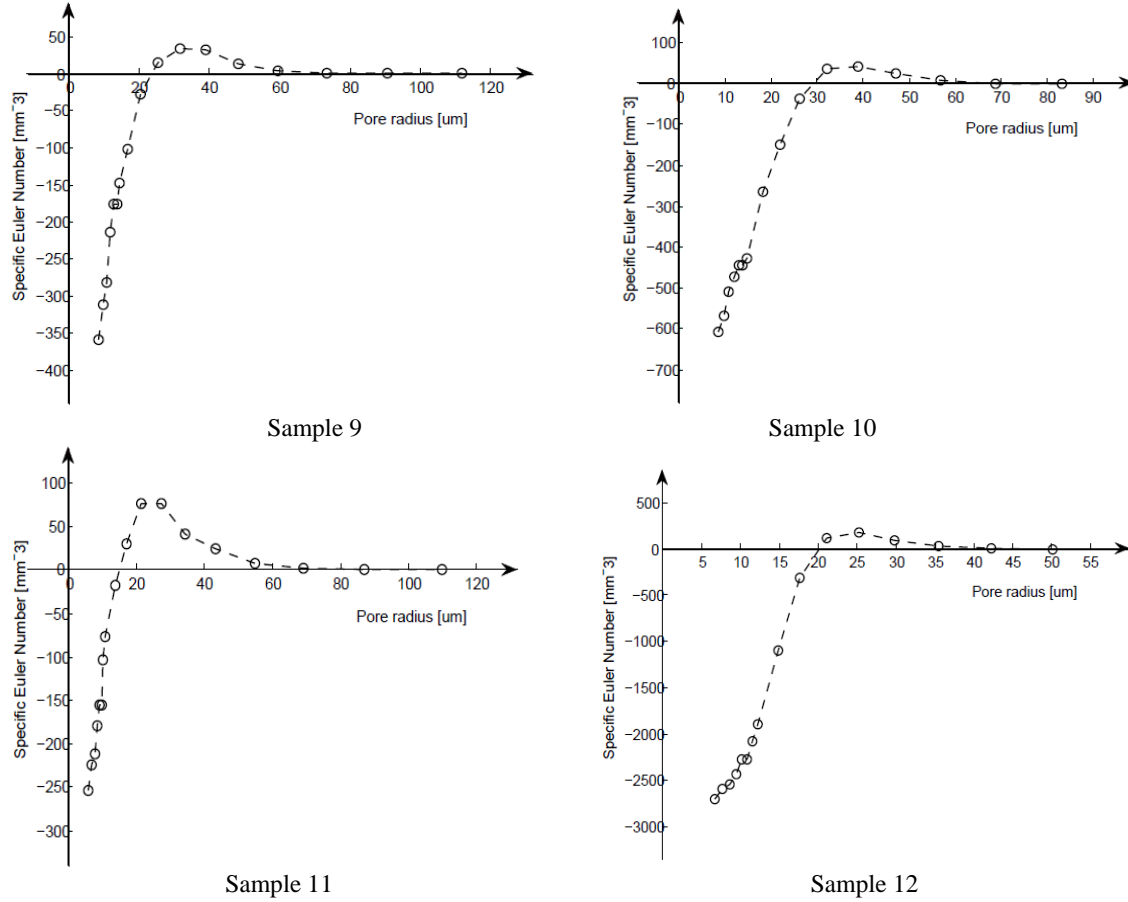


**Figure 5.** Connectivity function of 12 sandstone samples, the turning point (the zero crossing) is the critical pore size radius.

**Table 2** Sample data: Samples 1 and 2 have 400 voxels, which belong to Carbonate. The other samples have 300 voxels, which belong to Sandstone.  $r_m$  is the largest pore radii calculated by Eq.1,  $r_c$  is the zero crossing point of Connectivity functions,  $D$  is the fractal dimension calculated by Eq.11,  $p_c$  is the percolation threshold calculated by Eq.14,  $p_c^*$  is the percolation threshold calculated by Eq.20, the specific Euler number calculated by Jiang(2011).

Sample	$k_{LB}(\text{um}^2)$	$\phi$	$r_0[\text{um}]$	$r_m(\text{um})$	$r_c[\text{um}]$	$D$	$p_c(\text{Eq.14})$	$p_c^*(\text{Eq.20})$	$\chi_V(\text{um}^{-3})$
1	1.09	0.23	2.85	145.06	20.65	2.93	0.12	0.16	$-5.83 \times 10^{-7}$
2	0.07	0.17	5.35	243.95	24.09	2.95	0.11	0.11	$-2.80 \times 10^{-8}$
3	1.66	0.14	8.68	280.36	20.00	2.96	0.11	0.11	$-4.55 \times 10^{-8}$
4	3.85	0.25	4.96	192.64	17.66	2.92	0.17	0.17	$-7.76 \times 10^{-7}$
5	0.22	0.17	9.10	312.11	14.58	2.95	0.15	0.13	$-2.59 \times 10^{-7}$
6	0.26	0.17	8.96	308.52	11.22	2.95	0.16	0.12	$-1.07 \times 10^{-7}$
7	4.59	0.21	4.00	147.62	51.80	2.93	0.07	0.12	$-1.53 \times 10^{-7}$
8	10.83	0.24	5.10	196.61	34.88	2.92	0.12	0.12	$-1.27 \times 10^{-7}$
9	6.87	0.25	4.80	187.95	22.42	2.92	0.15	0.15	$-5.06 \times 10^{-7}$
10	13.00	0.34	4.89	211.81	28.75	2.89	0.20	0.16	$-5.74 \times 10^{-7}$
11	2.19	0.22	3.40	127.64	16.15	2.93	0.13	0.14	$-3.39 \times 10^{-7}$
12	7.13	0.43	3.85	180.23	20.33	2.85	0.27	0.27	$-3.87 \times 10^{-6}$

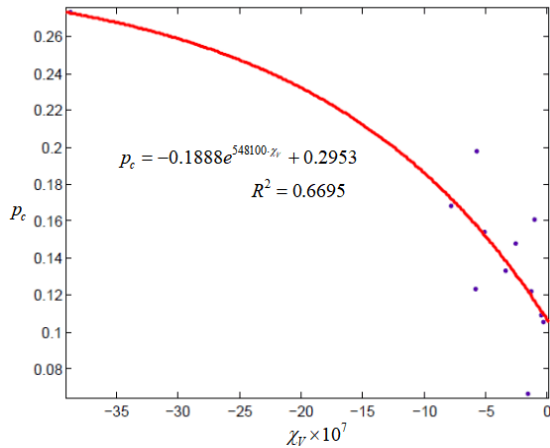


**Figure 6.** Percolation threshold as a function of the specific Euler number for all 12 samples.

**Table 3.** According to the data of Table 2, the permeability prediction value of pore medium is calculated by using different permeability prediction models, and the predicted values are compared with those obtained by LBM.  $k_{LB}$  is calculated by LBM,  $k_1$  is predicted permeability from Eq.17,  $k_2$  is predicted permeability from Eq.21. The data are shown in Figure 7.

Sample	$k_{LB}(\text{um}^2)$	$k_1(\text{um}^2)$	$k_2(\text{um}^2)$
1	1.09	2.36	2.21
2	0.07	1.70	1.69
3	1.66	0.81	0.81
4	3.85	1.78	1.76
5	0.22	0.58	0.60
6	0.26	0.34	0.37
7	4.59	13.39	12.13
8	10.83	7.17	7.20
9	6.87	3.06	3.08
10	13.00	8.84	9.47
11	2.19	1.28	1.27
12	7.13	6.47	6.47

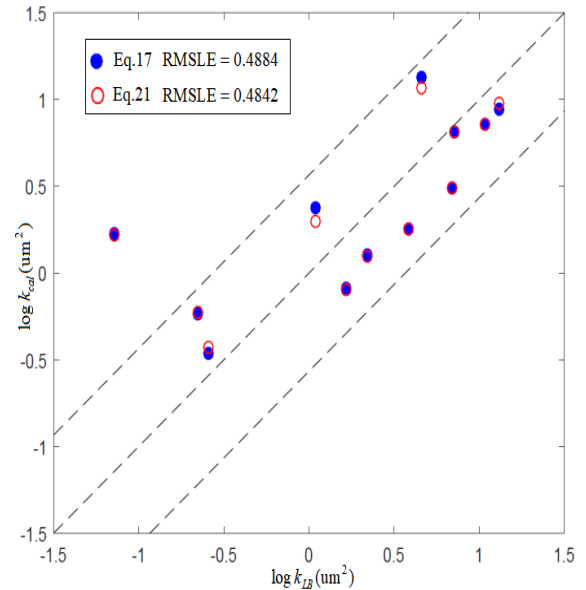


**Figure 7.** Logarithm of the permeability predicted from Eq.17, as well as logarithm permeability calculated from Eq.21 versus the measured one (calculated by LBM).  $k_{LB}$  is permeability calculated by LBM and  $k_{cal}$  is the calculated (estimated) permeability. The dotted line in the middle and the dashed lines on both sides represent the 1:1 line and the factor of three boundaries, respectively.

The permeability calculated using Eq.21 (RMSLE=0.4842) exhibits a better agreement than Eq.17 (RMSLE=0.4884). In order to draw a more reliable conclusion, all the permeability values calculated using Eq.21 are closely distributed along the  $y=x$  line in Figure 7, while the permeability calculated using Eq.17 deviate somewhat from the  $y=x$  line and this phenomenon becomes more obvious for samples with a low permeability. Because the porosity and pore radius of carbonate reservoir vary greatly and there are fracture phenomena, the permeability of most carbonate rock samples is not easy to predict. Therefore, it can be seen from the calculation results that the carbonate permeability calculated by Eq.21 (samples 1 and 2) is not accurate. However, the structural uniformity of sandstone is good, and the porosity and pore throat radius do not change much. Therefore, the accuracy of sandstone permeability calculated by using Eq.21 is high.

## 5 CONCLUSIONS

THIS study presents a new equation (Eq.21) that uses Euler Number and pore throat radii to estimate the permeability of porous media. Compared with the existing relations such as Eq.17, the new equation contains factors that reflect pore connectivity, and the form is simple and reliable. The results also show that the calculation of permeability from the critical pore size extracted from the connected function is in good agreement with the permeability measured by Ibm, and Eq .17 is also reliable. Although MICP has been studied for a long time, there are still some problems in the application process. For example, hysteresis (irreversibility between mercury intrusion and extrusion curves) and different contact angles between mercury and various porous media have attracted the attention of many researchers (Moro et al, 2002; Zhou et al, 2010). In this paper, we use the Connected Function to calculate the critical pore size of the porous media. With the collection of more rock data in the future, the new equation may be improved.

## 6 REFERENCES

- Bauget, F., Arns, C.H., Saadatfar, M., Turner, M.L., Sheppard, A.P., Sok, R.M., Pinczewski, V., Knackstedt, M.A., 2005. Rock typing and petrophysical property estimation via direct analysis on microtomographic images. In: Proceedings of International Symposium of the Society of Core Analysts, Toronto.
- Bauget, F., Arns, C.H., Saadatfar, M., Sheppard, A., Sok, R., Turner, M., Pinczewski, V., Knackstedt, M.A., 2005. What is the Characteristic Length scale for permeability? Direct analysis from microtomographic data. In: Proceedings of SPE Annual Technical Conference and Exhibition.
- Bear J. Dynamics of fluid in porous media. New York: Elsevier; 1972.
- Carman P.C., Fluid flow through granular beds. Trans Inst Chem Eng 1937; 15:150–67.
- Childs, E.C. Collis-George, N., 1950. The permeability of porous materials. In: Proceedings of the Royal Society of London, 201, pp. 392–405.
- Daigle, H., 2016. Application of critical path analysis for permeability prediction in natural porous media. Adv. Water Resour. 96, 43–54.
- Davud, D., Rouzbeh, G.M., (2018). Impact of pore compressibility and connectivity loss on shale permeability. International Journal of Geology, 187:98-113.
- Davudov, D., Moghanloo, R.G., Yuan, B., 2016, August. Impact of pore connectivity and topology on gas productivity in Barnett and Haynesville shale plays. In: Unconventional Resources Technology Conference, San Antonio, Texas, 1-3 August 2016. Society of Exploration Geophysicists, American Association of Petroleum Geologists, Society of Petroleum Engineers, pp. 2790–2806.
- Davudov, D., Moghanloo, R. G., Lan, Y. et al. 2017. Investigation of Shale Pore Compressibility Impact on Production with Reservoir Simulation. Presented at the SPE Unconventional Resources Conference, Calgary, 15–16.
- Dullien, F. A. L., 1992. Porous Media: Fluid Transport and Pore Structure. Academic Press, New York.
- Ganesh M., Naresh M., & Arvind C. (2017) MRI Brain Image Segmentation Using Enhanced Adaptive Fuzzy K-Means Algorithm, Intelligent Automation & Soft Computing, 23(2), 325-330.
- Ghanbarian, B., Hunt, A.G., Ewing, R.P., Skinner, T.E., 2014. Universal scaling of the formation factor in porous media derived by combining percolation and effective medium theories. Geophys. Res. Lett. 41 (11), 3884–3890.
- Friedman, S.P., Seaton, N.A., 1998. Critical path analysis of the relationship between permeability and electrical conductivity of three-dimensional pore networks. Water Resour. Res. 34, 1703–1710.
- Gharsallah M. B., Mhammed I. B., & Braiek E. B. (2018). Improved Geometric Anisotropic Diffusion Filter for Radiography Image Enhancement, Intelligent Automation & Soft Computing, 24(2), 231-240.
- Hunt, A.G., 2001. Applications of percolation theory to porous media with distributed local conductances. Adv. Water Resour. 24 (3), 279–307.
- Hunt, A. G., and R. P. Ewing (2009), Percolation theory for flow in porous media, Lect. Not. Phys., 2nd ed., pp. 771, Springer, Berlin.
- Hunt, A. G., Ewing, R., 2014. Percolation theory for flow in porous media, Springer, 3rd ed.
- Marshall, T.J., 1957. Permeability and the size distribution of pores. Nature 180, 664-665.
- Marshall, T.J., 1958. A relation between permeability and size distribution of pores. J. Soil Sci. 9 (1), 1–8.
- Moro, F. and Böhni, H., 2002. Ink-Bottle Effect in Mercury Intrusion porosimetry of Cement-Based materials J. Colloid Interface Sci.246:135-149.
- Mulder, M., Transport in porous membranes. Porous membranes for microfiltration and ultrafiltration. Casting of membranes and methods for determination of their properties, Lecture on School Membranes and Membrane Separation Techniques of Joint European Network in UMK, JEN-04720- PL-95, Torun, 23±29 June 1996.
- Knackstedt, M.A., Arns, C.H., Bauget, F., Sakellariou, A., Senden, T.J., Sheppard, A.P., Sok, R.M., 2006. Quantitative transport properties of granular material calculated from X-ray CT images. Advances in X-ray Analysis, 49, 92-97.
- Kaviany M. Principles of heat transfer in porous media. 2nd ed. New York: Springer; 1995.
- Katz, A.J., Thompson, A.H., December, 1986. Quantitative prediction of permeability in porous rock. Phys. Rev. B 34 (11), 8179–8181.

- Katz, A.J., Tompson, A.H., 1987. Prediction of rock electrical conductivity from mercury injection experiments. *J. Geophys. Res.* 92, 599–607.
- Kong, T. Y., Digital topology: Introduction and survey”, *Computer Vision, Graphics and Image Processing*, vol.48 , no.3,pp.357-393, 1989.
- Kozeny J. Ueber kapillare Leitung des Wassers im Boden. *Stizungsber Akad Wiss Wien* 1927;136:271–306.
- Liu C. J., Wu X. L., Mo B. & Zhang Y., 2018. Multi-phase Oil Tank Recognition for High Resolution Remote Sensing Images, *Intelligent Automation & Soft Computing*, 24(3), 663-670.
- Mandelbrot, B.B., *The Fractal Geometry of Nature*, W.H. Freeman, New York, 1982, pp. 23–57.
- Pape, H., Clauser, C., Iffland, J., 2000. Variation of permeability with porosity in sandstone diagenesis interpreted with a fractal pore space model. *Pure Appl. Geophys.* 157, 603–619.
- Purcell, W.R., 1949. Capillary pressures-their measurement using mercury and the calculation of permeability therefrom. *J. Pet. Technol.* 1 (2), 39–48.
- Robins, V., M. Saadatfar, O. Delgado-Friedrichs, and A. P. Sheppard (2016), Percolating length scales from topological persistence analysis of micro-CT images of porous materials, *Water Resour. Res.*, 52, 315–329.
- Saha, P. K. and Chaudhuri, B. B., 1995. A new approach to computing the Euler characteristic, *Pattern recognition*, 28(12), 1955-1963.
- Skaggs, T.H., 2011. Assessment of critical path analyses of the relationship between permeability and electrical conductivity of pore networks. *Adv. Water Resour.* 34, 1335–1342.
- Ghanbarian, B., Hunt, A.G., Ewing, R.P., Skinner, T.E., 2014. Universal scaling of the formation factor in porous media derived by combining percolation and effective medium theories. *Geophys. Res. Lett.* 41, 3884–3889.
- Ghanbarian, B., Hunt, A.G., Skaggs, T.H., Jarvis, N., 2017. Upscaling soil saturated hydraulic conductivity from pore throat characteristics. *Adv. Water Resour.*, 104, 105–113.
- Giesche H. Mercury porosimetry: a general (practical) overview. *Part. Part. Syst. Charact.* 2006, 23, 9–19.
- Hugh Daigle, Relative permeability to water or gas in the presence of hydrates in porous media from critical path analysis, *Journal of Petroleum Science and Engineering*, 146(2016), 526-535.
- Jiang, Z., Wu, K. and Couples, G., et al, 2007. Efficient extraction of networks from three-dimensional porous media, *Water resources research*, 43, 1-17.
- Jiang, Z., Wu, K., Couples, G., 2011. Characterisation of pore sizes and connectivity in 3d porous media, *CMWRXVI*.
- Jiang, Z., Van Dijke, M. I. J., and Wu, K., et al, 2012. Stochastic Pore Network Generation from 3D Rock Images, *Transport in porous media*, 94(2), 571-593.
- Scholz, C., Wirner, F., Götz, J., Rüde, U., Schröder-Turk, G. E., Mecke, K., and Bechinger, C., Permeability of Porous Materials Determined from the Euler Characteristic, *Phys. Rev. Lett.* 109, 264504 (2012).
- Stauffer, D., Aharony, A., 1992. *Introduction to Percolation Theory*, Second ed. Taylor and Francis, London.
- Tyler, S.W., Wheatcraft, S.W., 1990. Fractal processes in soil water retention. *Water Resour. Res.* 26, 1047–1054.
- Vogel H.J., A numerical experiment on pore size, pore connectivity, water retention, permeability, and solute transport using network models. *Eur J Soil Sci* 2000; 51:99–105.
- Vogel H.J., Roth, K. Quantitative morphology and network representation of soil pore structure. *Adv Water Resour* 2001; 24:233–42.
- Washburn E. W., Note on a method of determining the distribution of pore sizes in a porous materials. *Proc Natl Acad. Sci.* 1921, 7(4), 115-116.
- Zhao, H.Q., Macdonald, I.F., Kwiecie, M.J., 1994. A necessity in the identification of pore necks in porous media by 3D computer reconstruction from serial section data. *Journal of colloid and interface science*, 162(2), 390-401.
- Zhou, J., Ye, G. and Breugel, K., 2010. Characterization of pore structure in cement-based materials using pressurization–depressurization cycling mercury intrusion porosimetry (PDC-MIP), *Cem. Concr. Res.* 40:1120-1128.

## 7 NOTES ON CONTRIBUTORS



**Zhao Yibo** received the B.S. degree with distinction in Department of Mathematics from Heze University, Shandong, China, in 2008, the M.Sc. degree in School of Mathematics and Physics from University of South China, Hunan, China, in 2010. In 2016, he was admitted to the school of Mathematics Sciences of the University of Electronic Science and Technology of China to pursue his Ph.D. Now he is a lecturer at Shandong Women's University. His current research interests include image processing, porous media, and seepage model.